Electrical admittance of piezoelectric parallelepipeds: application to tensorial characterization of piezoceramics

Oumar Diallo, Emmanuel Le Clezio, Thomas Delaunay, M. Bavencoffe, Guy Feuillard

Electrical admittance of piezoelectric parallelepipeds: application to tensorial characterization of piezoceramics

Cite as: AIP Advances **4**, 017121 (2014); https://doi.org/10.1063/1.4863090
Submitted: 08 October 2013 . Accepted: 06 January 2014 . Published Online: 23 January 2014

O. Diallo, E. Le Clezio, T. Delaunay, M. Bavencoffe, and G. Feuillard

Electrical admittance of piezoelectric parallelepipeds: application to tensorial characterization of piezoceramics

O. Diallo,[1] E. Le Clezio,[2] T. Delaunay,[2] M. Bavencoffe,[1] and G. Feuillard[1]
[1]*Laboratoire GREMAN UMR CNRS 7347. École Nationale d'Ingénieurs du Val de Loire Université François Rabelais de Tours 3 Rue de la Chocolaterie BP 3410 41034 BLOIS CEDEX France*
[2]*Institut d'Electronique du Sud UMR CNRS 5214 IES - MIRA case 082Université Montpellier 2 Place Eugène Bataillon 34095 MONTPELLIER CEDEX 5 France*

(Received 8 October 2013; accepted 6 January 2014; published online 23 January 2014)

This work deals with the characterization of functional properties, including determination of mechanical and electrical losses, of piezoelectric materials using only one sample and one measurement. First, the natural resonant frequencies of a piezoelectric parallelepiped are calculated and the electrical admittance is determined from calculations of the charge quantity on both electrodes of the parallelepiped. A first validation of the model is performed using a comparison with Mason's model. Results are reported for a PMN-34.5PT ceramic cube and a good agreement is found between experimental admittance measurements and their modeling. The functional properties of the PMN-34.5PT are then extracted. [http://dx.doi.org/10.1063/1.4863090]

I. INTRODUCTION

Ultrasonic Resonance Spectroscopy allows the characterisation of piezoelectric materials thanks to the study of their mechanical and electrical resonances.[1–5] This method examines the vibration modes of a piezoelectric cube and relates mechanical resonances to electromechanical properties.[2–4,6–9] Taking advantage of the inverse piezoelectric effect, Delaunay *et al.*[3] proposed an ultrasonic characterization method of ceramic cubes with a experimental set-up based on vibration measurements thanks to Laser interferometry. This method is here modified to obtain the electromechanical properties of piezoelectric ceramics from electrical measurements only. Properties are deduced from the study of the electrical admittance of the sample. First, following the approach adopted by Holland and Nisse,[10] the eigen frequencies and eigen modes of a piezoelectric cube with electrodes on two faces are calculated. The calculation of the charge quantity on these two electrodes is then expressed and allows the electrical admittance to be calculated. Experimental admittance measurements on a PMN-34.5PT piezoceramic cube are carried out and compared to theoretical calculations. In addition, the symmetry of electrical vibration modes is identified by laser interferometry using a wide band excitation. These results are discussed and the validity of the method is demonstrated. Finally, functional properties of the PMN-34.5 PT piezoceramic are extracted and compared to the data published in the literature.

II. ADMITTANCE OF A PIEZOELECTRIC PARALLELEPIPED SAMPLE

A. Resonant frequencies

Consider the piezoelectric parallelepiped presented in Figure 1. Its dimensions are $2L_1$, $2L_2$ and $2L_3$ and the origin of the axes is taken at the center of the sample. The top and bottom faces $x_3 = L_3$ and $x_3 = -L_3$ are metalized and normal to the material polarization axis.

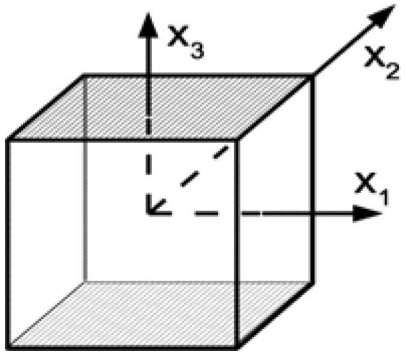

FIG. 1. Piezoelectric parallelepiped with dimensions $2L_1$, $2L_2$ and $2L_3$ poled along x_3.

To compute the electrical admittance of the piezoelectric element, the vibration eigenmodes of the parallelepiped are first identified thanks to the procedure proposed in.[3] The system's stationary points are sought by minimizing the Lagrangian where the mechanical displacements, $\overrightarrow{u_i}$, and the electrical potential, ϕ, inside the sample are expressed through the Rayleigh-Ritz method as a linear combination of trial functions $\overrightarrow{\psi_p}$ and φ_r:

$$\overrightarrow{u_i} = \sum_{p=1}^{N} a_p \overrightarrow{\psi_p} \tag{1}$$

$$\phi = \sum_{r=1}^{M} b_r \varphi_r \tag{2}$$

where coefficients a_p and b_r are obtained by calculating the stationary points of the Lagrangian. Minimization of the Lagrangian leads to an eigen values system whom eigenvector are the coefficients a_p and b_r and whom eigenvalues are the resonant frequencies of parallelepiped.

To take into account the two electrodes, they are here modified to correspond to the short circuit or zero potential boundary condition on the metalized faces. Although this is not a necessary condition, it increases the computation convergence and simplifies the calculation of the interaction matrices. The proposed basis functions of displacement and electrical potential are respectively:

$$\overrightarrow{\psi_p} = \frac{1}{\sqrt{L_1 L_2 L_3}} P_\lambda\left(\frac{x_1}{L_1}\right) P_\mu\left(\frac{x_2}{L_2}\right) P_\nu\left(\frac{x_3}{L_3}\right) \overrightarrow{e_i} \tag{3}$$

$$\phi_r = \frac{1}{\sqrt{L_1 L_2 L_3}} P_\xi\left(\frac{x_1}{L_1}\right) P_\zeta\left(\frac{x_2}{L_2}\right) f_\eta\left(\frac{x_3}{L_3}\right) \tag{4}$$

with

$$f_\eta\left(\frac{x_3}{L_3}\right) = (-1)^\eta \left(1 - \frac{x_3}{L_3}\right) P_\eta\left(\frac{x_3}{L_3}\right) \tag{5}$$

The p^{th} and r^{th} basic functions ψ_p and ϕ_r are defined by the triplets, (λ, μ, ν) and (ξ, ζ, η), respectively. $P_\alpha(x)$ is the normalized Legendre function of order α and $\overrightarrow{e_i}$ is the unit displacement vector in x_1 direction, $\frac{1}{\sqrt{L_1 L_2 L_3}}$ is a normalization term.[2,4,5]

B. Calculation of electrical admittance

Once the evolution of the mechanical displacement and the electrical potential are known for each resonance frequency, the free charge, $Q^{(p)}$, on one electrode p can be computed. This free

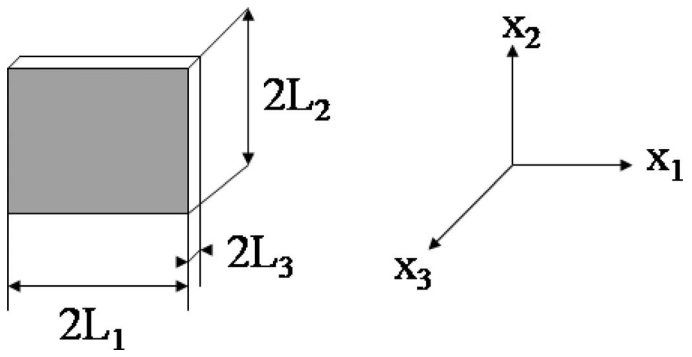

FIG. 2. Piezoelectric parallelepiped with dimensions $2L_1 = 2L_2 \gg 2L_3$ and poled along x_3.

charge on the electrode p, is defined by:

$$Q^{(p)} = \iint_A \vec{N}_3 \left(e_{3kl} u_{k,l} - \varepsilon^S_{3n} \phi_{,n}\right) d\vec{A} \tag{6}$$

where e_{3kl} are the piezoelectric coefficients along the x_3 axis and ε^S_{3n} is the clamped dielectric constant along the x_3 axis. Indices k, l and n run from 1 to 3.

To calculate the admittance matrix formulas, it is necessary to express the short circuit current, I, between the top and the bottom electrode:

$$I = -j\omega \iint_A \vec{N}_3 \left(e_{3kl} u_{k,l} - \varepsilon^S_{3n} \phi_{,n}\right) d\vec{A} \tag{7}$$

where N_3 is the normal vector along x_3. The term in brackets represents the electrical displacement. The electrical admittance is given by the following expression:

$$Y = \frac{\partial I}{\partial \phi} \tag{8}$$

Performing the indicated differentiation on the current (Eq. (5)) leads to the electrical admittance matrix:[10,11]

$$Y = j\omega \sum_\mu \frac{Q^{(1)}_\mu Q^{(2)}_\mu}{\omega^2_\mu - \omega^2} + j\omega C^S \tag{9}$$

where μ is the number of the mode and C^S is the clamped capacitance between the top and the bottom electrode :

$$C^S = \varepsilon^S_{33} \frac{A}{2L_3} \tag{10}$$

C. Convergence criteria and validation of electrical admittance modeling

In order to study the convergence of this electrical admittance model, it will be compared to an existing one. Since here there is no 3-dimensionnal analytical model of electrical admittance found in the literature, the comparison will done using a 1-dimensionnal one, *i.e* Mason's model.[12] Figure 2 shows the considered sample for this validation study:

Mason's model determines the frequency evolution of the admittance (or impedance) of thin ceramic plates. According to this model the impedance of the plate which is presented in Figure 2 is expressed by:[13]

$$Z_{elec} = \frac{U}{I} = \frac{1}{jC_0\omega}\left[1 - k_t^2 \frac{\tan(kd/2)}{kd/2}\right] \tag{11}$$

TABLE I. Computed resonance and antiresonance of PMN34,5-PT plate ceramic.

Mason's Model	Antiresonances frequencies (f_a)	239290	717880	1196500	1675100
	$f_a/f_a(1)$	1	3	5	7
Variationnal Model	Antiresonances frequencies (f_a)	236600	716800	1200000	1893800
	$f_a/f_a(1)$	1	3	5	8

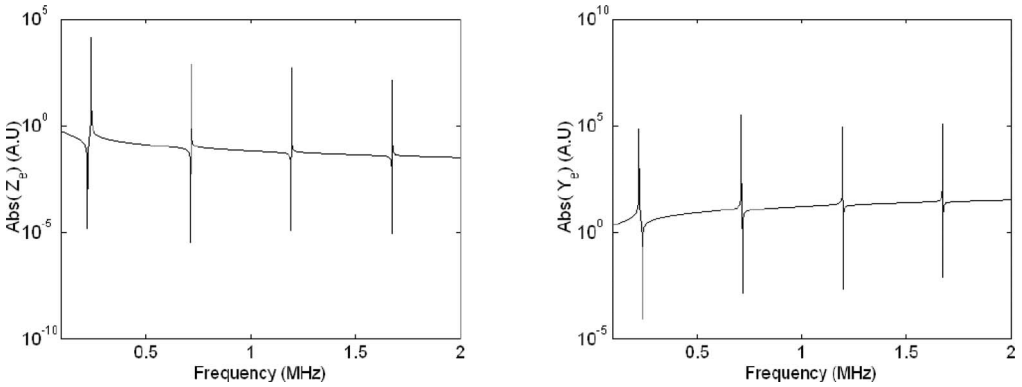

FIG. 3. Impedance and admittance of a PMN34,5-PT plate ceramic calculated with Mason's model.

The computation of this expression, using the values in section III and dimensions $2L_1 = 2L_3 = 1000$ mm against $2L_3 = 10$ mm, gives the electrical impedance and admittance spectra on Figure 3.

The peaks of the impedance spectrum are the antiresonance frequencies and the peaks of the admittance are the resonance frequencies. These frequencies are listed in the following table (Table I) and will be compared to those given by the variationnal admittance model.

Mason's model shows that only the odd harmonics of the antiresonance frequency are not null. The variationnal model (computed with $N = 9$) shows that the three first resonances are the same as those predicted by Mason's model. Only the odd harmonics are not null. However the fourth resonance is not correctly predicted by the two models. In this configuration, only thickness modes are predicted. Figure 4 shows that the predicted displacements at the face $x_3 = L_3$ for all the resonance frequencies indeed represent thickness modes.

For each one of frequencies, one can plot the particle displacements along $\mathbf{x_3}$ axis.

Figure 5 shows that the evolution of the particle displacements along x_3 is homogeneous to a $\sin(nx)$ where n is the number of the harmonic for the first three frequencies, but not for the fourth one. The resonance frequencies and antiresonance frequencies are different in piezoceramics. Because of the fourth resonance is not precisely predicted the resonance and the antiresonance frequencies are similar. This shows that the maximum degree for approximated Legendre polynomials taken in this study is only valid up to the 3th resonance.

If this computation is repeated with a higher degree, for instance with $N = 14$, the all four resonance frequencies from the two models fit perfectly. Figure 6 presents the obtained admittance and impedance spectra with $N = 14$ and it's comparison with results using Mason's model.

The agreement between the two models is satisfactory. If one wants to determine precisely the frequency of higher frequency harmonic, the maximum degree of Legendre polynomials needs to be increased. The antiresonance frequencies of the first three modes are unchanged only the fourth changed. In order to determine the degree in a frequency range we can calculate for many degrees and compare the given frequencies. If between two consecutives degrees the resonant frequencies are not changed the lower degree will be chosen because the computational time increases when the degree increases. This validates the convergence criteria and provides a first validation of our model.

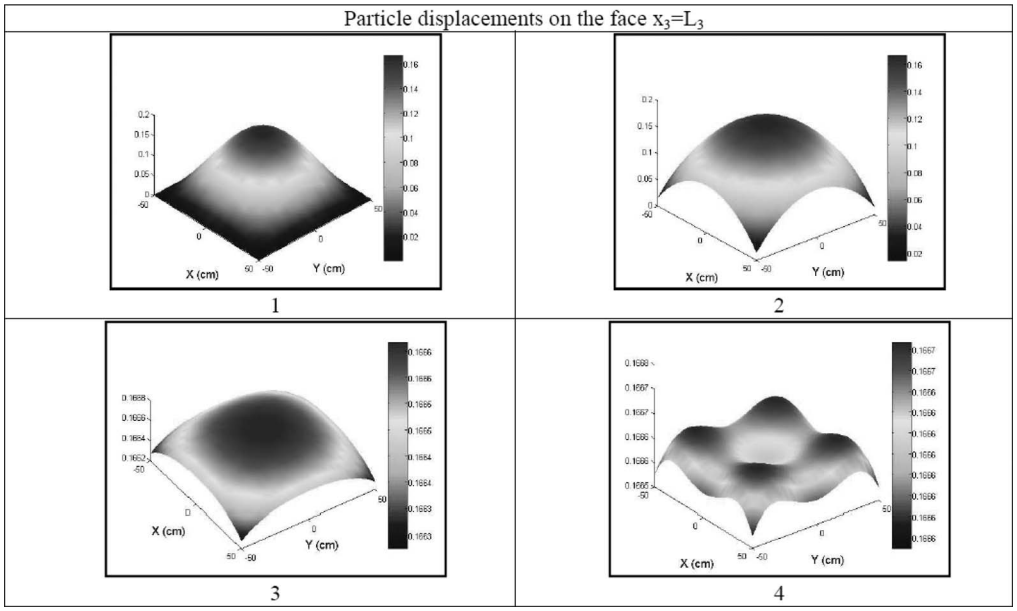

FIG. 4. Particle displacements calculated at the resonance frequency and its odd harmonics on face $x_3 = L_3$.

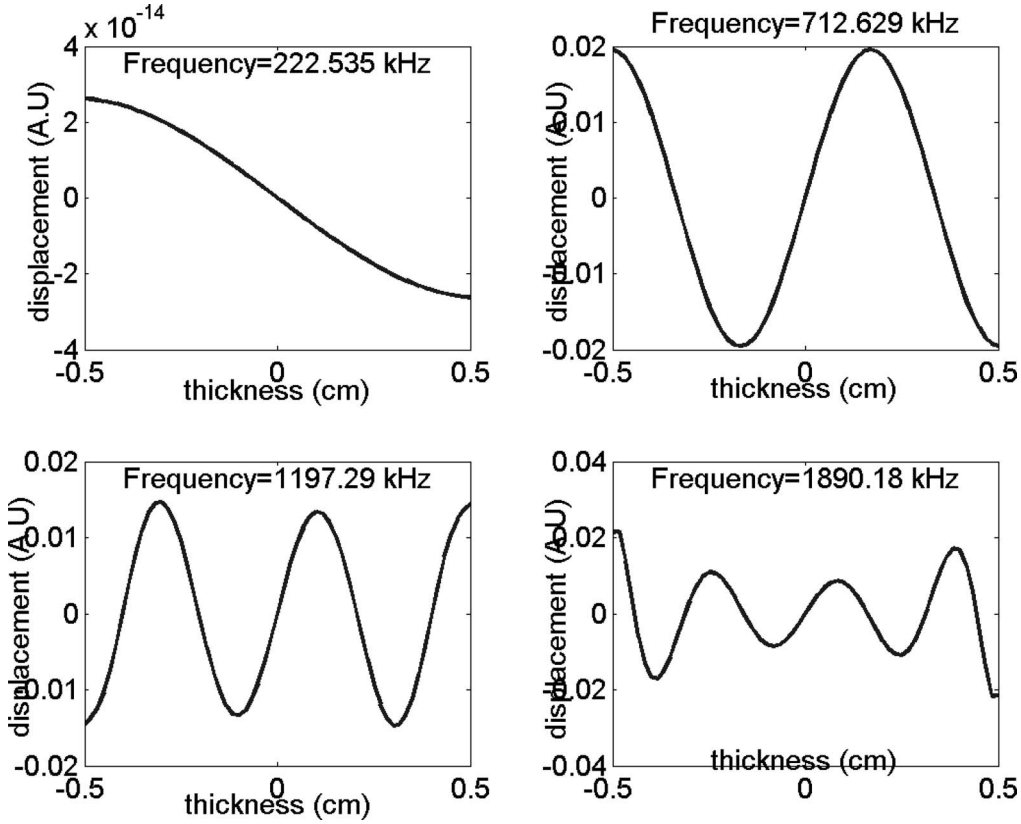

FIG. 5. Particle displacements calculated along $\mathbf{x_3}$ axis at the resonance frequency and its harmonics.

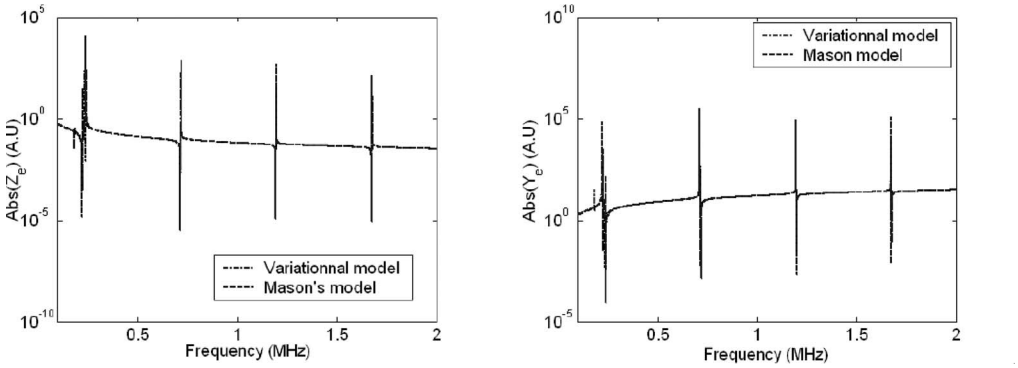

FIG. 6. Comparison between impedance and admittance of a PMN34.5PT plate ceramic calculated with Mason's model and with variationnal model (N = 14).

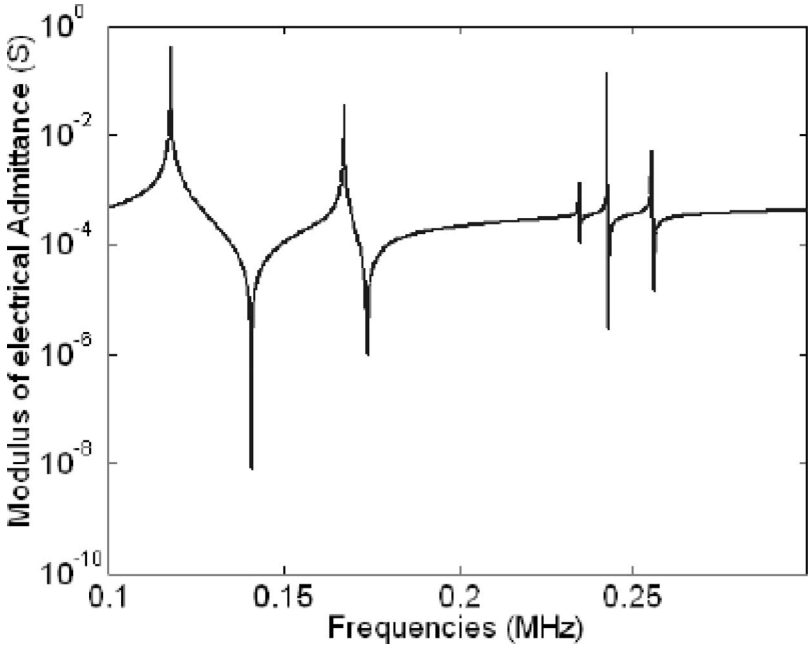

FIG. 7. Computed modulus of the electrical admittance of the PMN34.5PT cube.

D. Computation of the electrical admittance of a piezoceramic cube

The frequency evolution of the admittance of a $10 * 10 * 10$ mm^3 PMN-34.5PT piezoelectric cube computed from equation (6) is presented in Figure 7. The electromechanical characteristics of the material are taken from ref. 3.

In the considered frequency range, only five electrical resonances are observed; however the number of existing modes is much greater than five. The presence of electrodes on both sides of the piezoceramic cube drastically restricts the number of modes to those that are piezoelectrically coupled.

E. Admittance of a piezoelectric resonator with electrical and mechanical losses

Assuming viscous losses and dielectric losses in the ceramic, two dissipating energy terms appear in the expression of the Lagrangian of the system which must be subtracted from the total

energy. These dissipation terms can be rearranged to so that complex elastic and dielectric constants can be considered instead of real constants. Calculations are thus carried out considering a complex eigen value problem.

The mechanical losses are then introduced in the elastic tensor at constant electric field.[14]

$$\underline{C}^E = C^E (1 + j\delta_m) \tag{12}$$

Electrical losses are also introduced in the dielectric tensor at constant strain:

$$\underline{\varepsilon}^S = \varepsilon^S (1 + j\delta_{me}) \tag{13}$$

where, in both expressions, the tensorial notation was omitted for simplicity.

The mechanical displacement and electrical field have an imaginary part which is related to the damping of the material. The electrical admittance now has a real part also

$$Y = j\omega \sum_{\mu} \frac{\underline{Q}_{\mu}^{(2)}}{\underline{\omega}_{\mu}^2 - \omega^2} + j\omega \underline{C}^S \tag{14}$$

where $\underline{Q}_{\mu}^{(p)} = Q'^{(1)}_{\mu} + jQ''^{(p)}_{\mu} \cdot Q'^{(1)}_{\mu}$ is the charge quantity on the surface of the electrode and $Q''^{(p)}_{\mu}$ is a term including both mechanical and electrical losses that lead to a real part of the admittance.

III. EXPERIMENTAL RESULTS AND DISCUSSION

A PMN34.5PT piezoceramic sample with dimension $10 \times 10 \times 10$ mm^3 fully metalized on its top and bottom faces was characterized both electrically by impedance/admittance measurements and mechanically by laser measurements. Its properties are[3] $C_{11} = 174.7$, $C_{12} = 116.6$, $C_{13} = 119.3$, $C_{33} = 154.8$, $C_{44} = 26.7$, $C_{66} = 29$ in GPa; $e_{15} = 17{,}1$, $e_{31} = -6.4$, $e_{33} = 27.3$ in C/m^2; $\varepsilon_1 = 21.0105$, $\varepsilon_{33} = 25.0125$ in pF/m where elastic constants are at constant electric field and dielectric constants are at constant strain. They will be used as an initial guess tensor for the material's tensor.

A. Electrical admittance measurements

Electrical admittance measurements were carried out on an Omicron Bode 100 analyzer using a specific sample holder. The modulus of the admittance is presented in Figure 8.

Resonance frequencies and quality factor are determined from the admittance curve. Assuming that electric losses are weak which is the case in our ceramic sample, the quality factors, Q, of the electrical resonances are mainly related to mechanical losses $\delta_m = \delta = 1/Q$. Table II summarizes the theoretical and experimental resonance frequencies as well as the loss factor of each resonance. A sensitivity study of the resonance location to input parameters has shown that high frequency peaks were very sensitive to C_{66} and C_{33}. These C_{66} and C_{33} input values are close to the actual coefficients of the ceramics.

As for the theoretical admittance in Figure 7, which was calculated with real constants, five resonances are observed in the admittance curve (Figure 8) in the frequency range of analysis. The third resonance located at 239 kHz is very small; however its presence is confirmed by normal velocity measurements presented in the next section. Loss factor of this resonance was not determined because the signal to noise ratio (SNR) is not good. Experimental frequencies are slightly different from those measured by the Laser interferometer due to the fact that optimal transfer of energy is not necessarily located on the electrical resonant frequency.

The comparison between theoretical and experimental resonance frequencies shows that discrepancies on frequencies are low, the worst case being 7.24% for the first resonance. These discrepancies can be due to the fact that the constants used in the simulations do not exactly correspond to the electromechanical properties of our PMN34.5PT sample. The experimental resonances presented in Figure 8 are clearly affected in amplitude by the loss factors. They are not identical for all the peaks, as each mode does not involve the same weighting for piezoelastic coefficients.

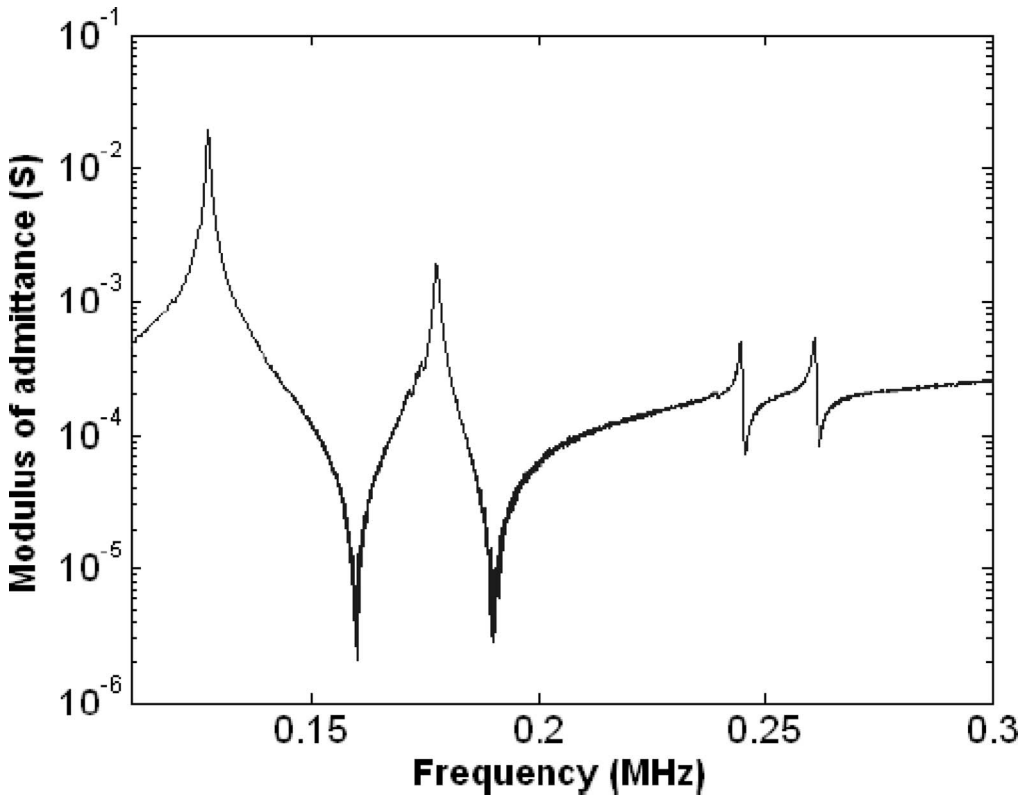

FIG. 8. Measured electrical admittance of PMN34.5PT cube.

TABLE II. theoretical (f_{th}) and experimental (f_{exp}) admittance resonant frequencies and mechanical losses of PMN-34.5PT cube.

Mode	1	2	3	4	5
Theoretical frequency, f_{th} (kHz)	117.7	167.3	234.6	242.7	255.4
Experimental frequency f_{exp} (kHz)	126.9	177.5	239.5	244.6	260.8
$(f_{exp} - f_{th})/ f_{exp}$ (%)	7.24	5.71	1.99	0.75	2.11
Mechanical losses(%)	0.5	0.9		0.9	0.3

In next section theoretical and experimental particle displacements at predicted resonance frequencies are compared in order to increase the confidence to our model.

Finally, dielectric losses were estimated from the quasi-static capacitance $Y = j\omega\underline{C}^S$ in equation (13):

$$Y = G + jB \tag{15}$$

where $G = \omega\delta_e C^S$ and $B = \omega C^S$. Outside of the resonances at 300 kHz, the determination of G gives a first estimation of the dielectric losses $\delta_e = 1{,}38 * 10^{-2}$.

B. Normal mode measurements

The normal particle displacements of the face $x_3 = L_3$ were measured using a Laser vibrometer (Polytech OFV-505). Resonant frequencies are identified and are associated to mode shapes. Figure 9 shows the experimental set up. The sample is set on a plastic holder and the electrical contact is ensured by a metallic strip fixed on a spring so that free mechanical boundary conditions at the surfaces of the cube are fulfilled. The piezoelectric cube is excited by a wide

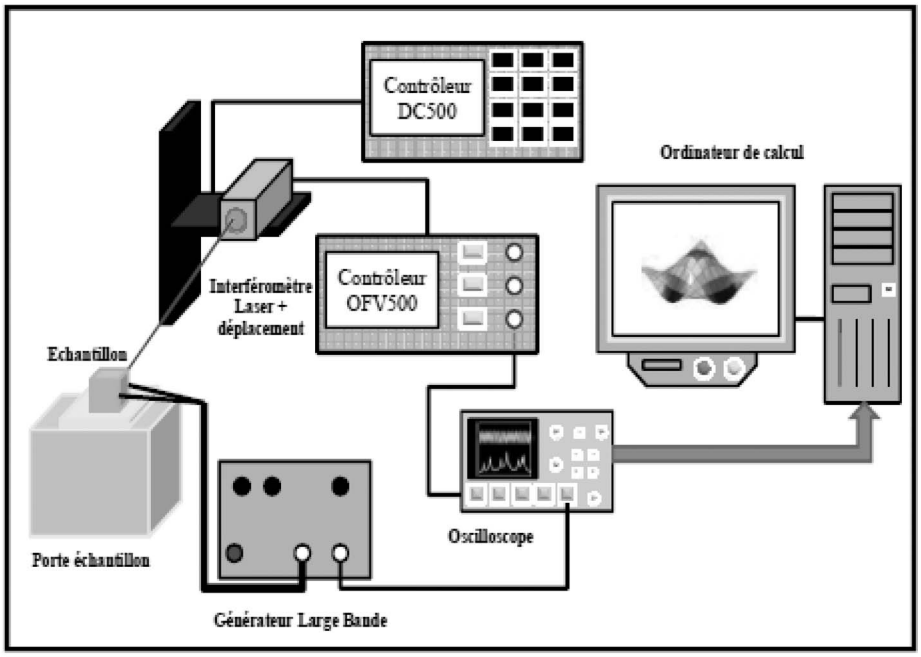

a)

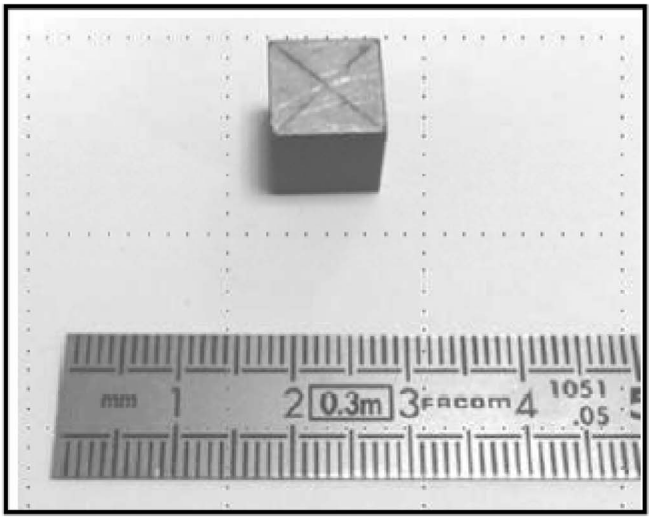

b)

FIG. 9. (a) Experimental set-up for laser vibration measurements, (b) ceramic sample.

band voltage pulser (Panametrics 5052 PR) to simultaneously excite all the coupled piezoelectric modes.

The interferometer is positioned at 50 cm from the sample. The velocity decoder sensitivity is either 5 mm/s/V or 25 mm/s/V, depending on the cut-off frequency, respectively 250 kHz and 1,5 MHz. The measured signals are sent to a computer via a digital oscilloscope. In the 100–300 kHz frequency range, the particle displacement exhibits many modes (see video) but only five are predicted by the admittance measurement. Figure 10 shows a comparison between theoretical

# mode	Computed face deformation	Measured face deformation
1	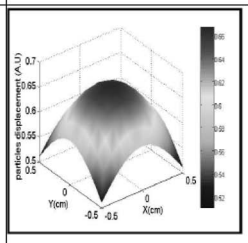	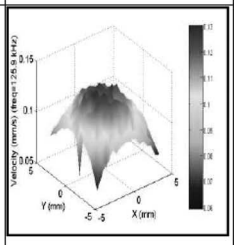
	117.7 kHz	126.1 kHz
2	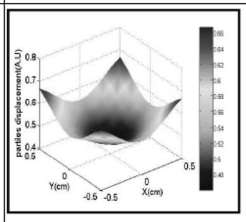	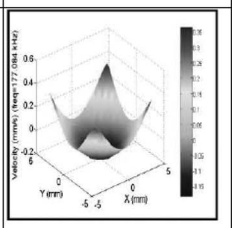
	167.3 kHz	177.5 kHz
3	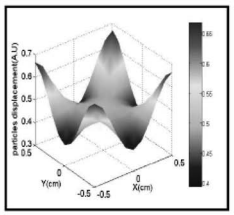	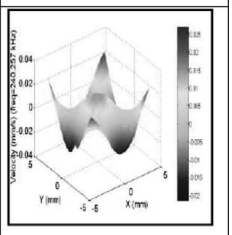
	234.6 kHz	240.1 kHz
4	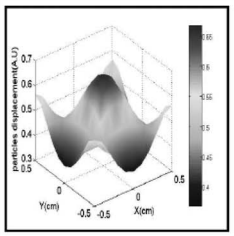	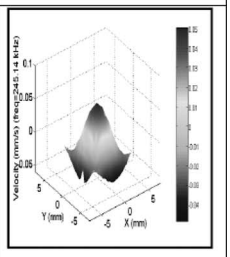
	242.7 kHz	245.4 kHz
5	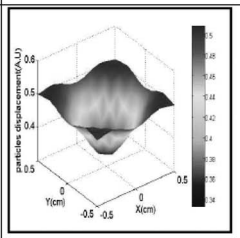	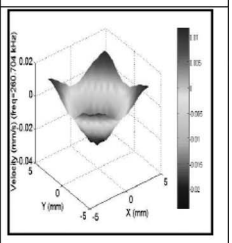
	255.4 kHz	262.1 kHz

FIG. 10. Computed and measured face deformation of the first five piezoelectrically coupled modes (enhanced). [URL: http://dx.doi.org/10.1063/1.4863090.1]

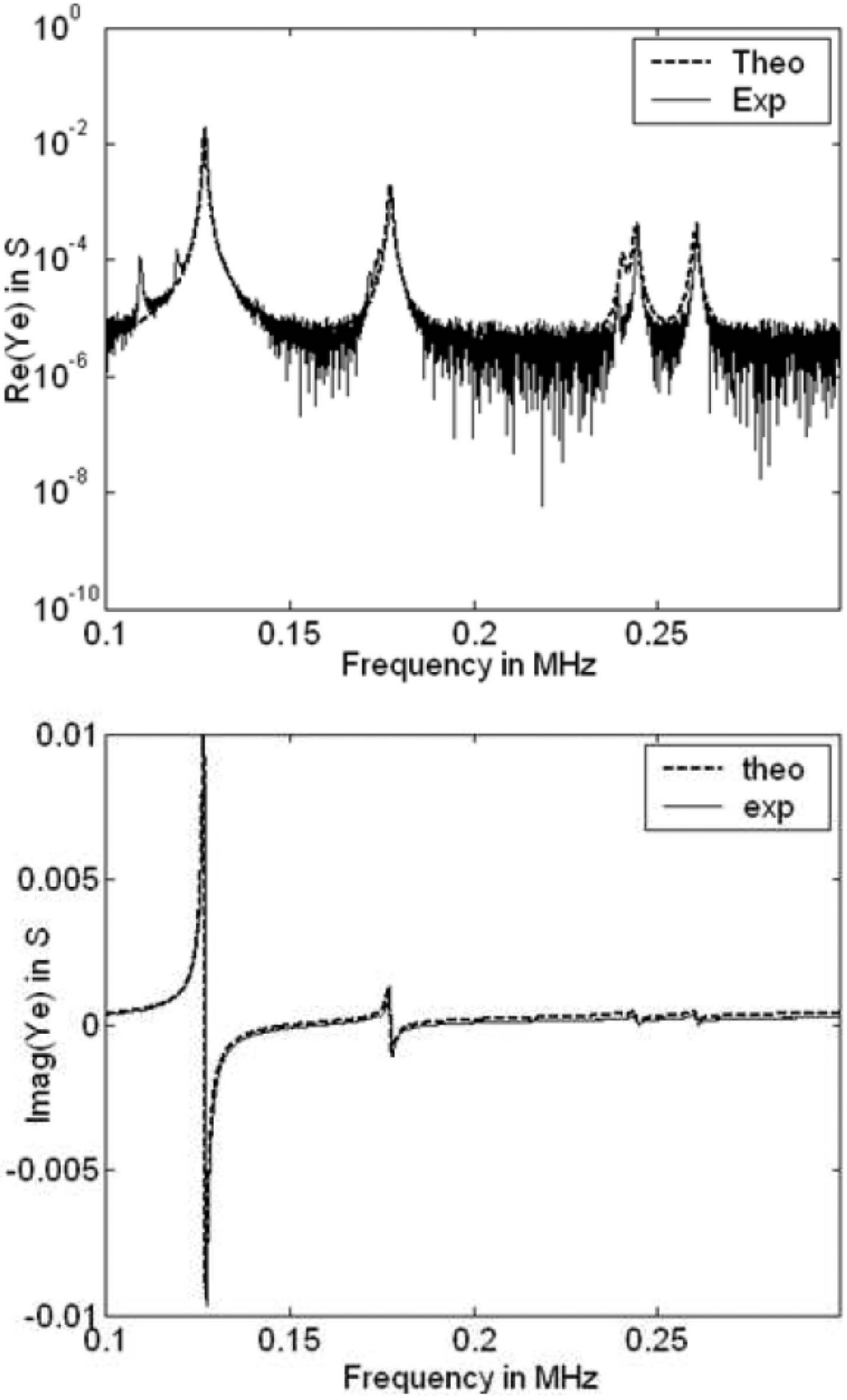

FIG. 11. Computed and measured electrical admittance.

TABLE III. Properties of a ceramic PMN 34,5PT deduced from the electrical admittance model.

Properties		Initial Values	Final Values	Units	Relative variation (%)
elastic	$C^E{}_{11}$	174.7	192.79	GPa	9.38
	$C^E{}_{12}$	116.6	136.2		14.38
	$C^E{}_{13}$	119.3	123.62		3.49
	$C^E{}_{33}$	154.8	156.96		1.38
	$C^E{}_{44}$	26.7	24.98		− 6.89
	$C^E{}_{66}$	29	28.27		− 2.58
dielectric	$\varepsilon^S{}_{11}$	21.0105	18.9646	nF/m	− 10.73
	$\varepsilon^S{}_{33}$	25.0125	23.5766		− 6.4
piezoelectric	e_{15}	17.1	17.24	C/m^2	0.81
	e_{31}	− 6.92	− 7.29		12.21
	e_{33}	27.3	28.76		5.08

and experimental particle displacements at the frequencies predicted by theoretical and experimental admittance. These measured modes shapes agree well with predicted ones.

In theory and in the experiments, the sample is electroded on the top and bottom faces which mean that a symmetrical excitation is applied. This should lead to the generation of centro-symmetric modes only, which is indeed confirmed on both theoretical and experimental results. The choice of basis functions (eq. (2)) with appropriate shape, *i.e.* zero potential on the top and bottom faces, increases the rapidity of the convergence towards the approximate solution. Here a degree equal to 7 for the trial function was used in the calculation.

Some discrepancies appear between theoretical and experimental frequencies. Their origin could lie in the values of the input piezoelectric tensor and in the values of loss factors.

IV. MATERIAL CHARACTERIZATION: EFFECTIVE PROPERTIES OF THE PMN-34.5PT

In this section material characteristics are determined assuming average mechanical and dielectric losses in the material. We have seen that taking into account the loss factor before piezoelastic constant determination is a crucial issue.

From the trial loss factor, dielectric and mechanical losses are fitted in order to have the same Q-factor, amplitude and threshold in the modelled electrical admittance as in the experimental admittance. After calculation one obtains $\delta_m = 5.4 * 10^{-3}$ and $\delta_e = 8.85 * 10^{-3}$. However, real piezoelastic constants have to be adjusted to properly locate the theoretical resonances, which will allow the determination of the piezoelastic properties. The piezoelastic tensor is then modified using a Simplex routine[15,16] so that theoretical admittance spectra is fitted to experimental one. The determination of the real part of the piezoelastic tensor is then deduced.

Results of the fitting are presented in Figure 11 on the real and imaginary parts of the admittance. The new data set of properties is given in Table III.

Looking at the comparison between our calculated piezoelastic tensor and the original data set, elastic parameters C_{11}, C_{12}, ϵ_{11} and e_{31} are higher than the original ones, while other properties are close to the initial values. This can be explained by the fact that original properties were determined from the same sample but with a single metallised face and it has been observed that electrical boundary conditions strongly affect these constants.

V. CONCLUSION

In this paper we have studied the eigen-vibration modes of piezoelectric cubes. We have calculated the electrical admittance of the cube and shown that electrical boundary conditions strongly influence the piezoelectrically coupled modes. In the frequency bandwidth of the study, there is a good agreement between the theoretical and experimental particle displacements at the surface of the studied cube. However, resonance frequencies are not located exactly at the expected values

due to their strong sensitivity to the material electromechanical parameters. We have introduced electrical and mechanical losses in order to compute the amplitude of the admittance and quantify their influence on the resonances. Then, the inverse problem was solved to identify the properties of the material and the new tensor is compared to initial estimations.

In further studies we plan to:

- extend this method to other ceramics(PZ52PT,..),
- extend this method to other shapes(cylinder. . .),
- determine the effect of the size of electrodes on the piezoelectrically coupled resonances.

[1] I. Ohno, J. Phys. Earth **24**, 355–379 (1976).
[2] I. Ohno, Phys. Chem. Minerals **17**, 371–378 (1990).
[3] T. Delaunay, E. L. Clezio, M. Guennou, H. Dammak, M. P. Thi, and G. Feuillard, IEEE transactions on ultrasonics, ferroelectrics, and frequency control **55**(2), 476–88, Feb. (2008).
[4] H. H. Demarest, The Journal of the Acoustical Society of America **49**(3B), 768 (1971).
[5] W. M. Visscher, A. Migliori, T. M. Bell, and R. A. Reinert, The Journal of the Acoustical Society of America **90**(4), 2154 (1991).
[6] A. Migliori, J. L. Sarrao, W. M. Visscher, T. M. Bell, M. Lei, Z. Fisk, and R. G. Leisure, Physica B: Condensed Matter, **183**(1–2), 1–24 (1993).
[7] S. J. Reese, K. L. Telschow, T. M. Lillo, and D. H. Hurley, IEEE transactions on ultrasonics, ferroelectrics, and frequency control **55**(4), 770–7 (2008).
[8] F. Farzbod and D. H. Hurley, IEEE transactions on ultrasonics, ferroelectrics, and frequency control **59**(11), 2470–5 (2012).
[9] D. Sancho-Knapik, H. Calas, J. J. Peguero-Pina, A. Ramos Fernandez, E. Gil-Pelegrin, and T. E. G. Alvarez-Arenas, IEEE Transactions on Ultrasonics, Ferroelectrics and Frequency Control **59**(2), 319–325 (2012).
[10] R. Holland and E. P. EerNisse, IEEE Transactions on Sonics and Ultrasonics **15**(2), 119–131 (1968).
[11] R. Holland, The Journal of the Acoustical Society of America **43**(5), 988 (1968).
[12] W. P. Mason, *Electromechanical transducers and wave filters*, 2nd Edition, Vol. 72, no. 10. 1948.
[13] D. Royer and E. Dieulesaint, *Ed.* Masson. (Paris, 1999), p. 410.
[14] V. Loyau, PhD Thesis Université François Rabelais de TOURS, 2004.
[15] J. A. Nelder and R. Mead, Oxford Journals (1965).
[16] E. Zahara and Y.-T. Kao, Expert Systems with Applications **36**(2), 3880–3886 (2009).